Materials Research. 2014; 17(6): 1477-1484
DOI: http://dx.doi.org/10.1590/1516-1439.204713

Numerical Investigation of Sliding Frictional Contact in Functionally Graded Steels (FGS)

Seyed Ali Sadough Vanini[a], Mohamad Shahba[b], Naser Kordani[a,b]*

[a]*Department of Mechanical Engineering, Amirkabir University of Technology, Tehran, Iran*
[b]*Department of Mechanical Engineering, Mazandaran University, Mazandaran, Iran*

Received: May 4, 2013; Revised: July 24, 2014

This study will analyze the two-dimensional nonlinear partial slip contact problem between a graded half plane in the normal to the contact interface and a rigid flat punch subject to a normal load. The problem, formulated under plane strain conditions, is reduced to singular integral equations of the second kind that are then solved with an expansion–collocation technique. A parametric analysis is carried out to assess the effect of friction coefficient on contact stresses, stress intensity factors and failure loads. The analytical model is in close agreement with finite element simulations. Remarkably, the graded constructions allow the critical load to be increased by two times with respect to common austenitic and ferrite steels.

Keywords: *functionally graded steels, singular integral equations, stress intensity factors, finite element method*

1. Introduction

There is an extensive literature on functionally graded materials (FGMs)[1]. Many applications of FGM arise in ceramic–metal systems and in traditional systems such as carburized steels used to improve a specific property such as wear resistance. However the possibility of using a simple geometric arrangement of compositionally graded phases in metallic systems enables materials to be designed to control a range of plastic properties and fracture processes[2].

The fabrication process of FGMs is a quite complex task. In this sense, most published works deal with laminated samples that are formed by homogeneous layers of different compositions. On the contrary, continuous FGMs are scarcely reported. An extraordinary effort has been made in order to develop continuous FGMs in a wide range of systems and it has been attained in several works[3]. In this way, functionally graded steels (FGSs) have recently been produced from austenitic stainless steel and carbon steel using electro slag refining (ESR)[4,5]. In these composites, by selecting the appropriate arrangement and thickness of the primary ferritic and austenitic steels as electrodes, it is possible to obtain composites with several layers consist of ferrite, austenite, bainite and martensite. The resultant composites using two slices of original ferrite (α_0) and original austenite (γ_0) is as below;

$$(\alpha_0\gamma_0)_{el} \overset{R}{\rightarrow} (\alpha\beta\gamma)_{com}$$

Where α, β and γ are ferrite, bainite and austenite phase in the final composite respectively; el is electrode; com is composite and R is remelting.

Diffusion of chromium, nickel and carbon atoms which taking place at the remelting stage in the liquid phase controls the chemical distribution of chromium, nickel and carbon atoms in the produced composites. The thicknesses of the bainitic and martensitic layers depend on the thickness of the corresponding primary slices in the electrode and process variables (voltage, current intensity and the drawing velocity of the product). The transformation characteristics of FGSs have previously been investigated, in that the diffusion coefficients of chromium, nickel, and carbon atoms at temperatures just above the melting point of iron were estimated.

Also, the thicknesses of the emerging bainite and martensite phases were determined[4].

Furthermore it has been shown that the tensile strength of the FGS composites depends on the composition and number of layers and those has been modeled based on the tensile behavior of individual phases[5]; to do so the yield stress of each layer in the composites was related to the microhardness value of that layer.

In the previous studies, Charpy impact energy of functionally graded steels in crack divider configurationand in crack arrester configuration[6] was experimentally examined and modeled by different methods. Fracture toughness of these specimens in terms of J_{IC} in both crack divider and crack arrester[7] configurations was also investigated. The tensile behavior of oblique layer functionally graded steels was the other property which studied in the previous studies[8,9]. Prediction Vickers hardness[10] and tensile strength[11] of functionally graded steels by the mechanism-based strain gradient plasticity theory was the other works done in this area.

Although there is an extensive volume of literature on contact mechanics of functionally graded materials, there seems to be only a few studies investigating the behavior of cracks located in FGMs subjected to contact stresses[12-14]. Through experiments conducted on graded specimens,[12] showed that a controlled gradient in the modulus of elasticity at a surface could eliminate conical cracking that results from Hertzian indentation. Choi considered a nonhomogeneous medium that comprises a homogeneous substrate, a graded

*e-mail: naser.kordani@gmail.com

interfacial layer, and a homogeneous coating[13]. By assuming that the composite medium is under the effect of contact stresses, the author computed the stress intensity factors (SIFs) for an embedded crack in the homogeneous substrate by using an analytical method. analytical technique based on the singular integral equations (SIEs) to evaluate mode I and II SIFs for a surface crack lying in a graded half-plane, that is in contact with a sliding flat stamp[14].

The analytical model considers a FGS half-plane with a crack, in contact with a rigid flat punch. The crack develops in the direction normal to the contact interface, in the same direction of grading. Such crack divider configuration was introduced by Aghazadeh et al.[15].The shear modulus of the half-plane is assumed to constant along the lateral direction. The problem is reduced to a system of singular integral equation of the second kind which is solved numerically to compute the contact stress distributions. In order to provide more insight into the behaviour of the functionally graded steel, contact mechanics analysis is also conducted by means of the finite element method. The parametric analyses are performed by considering flat punch profiles. The presented results illustrate the influences the coefficient of Coulomb friction on the distributions of the contact stresses and stress intensity factors.

2. Analytical Solution

The geometry of the considered contact /crack problem is depicted in Figure 1. The contact area extends from x= a to x = b at the surface y = 0. Coulomb's dry friction law is assumed to hold in the contact area hence the tangential force per unit length Q transferred by the contact is taken to be equal to ηP where η is the coefficient of friction and P is the applied normal force per unit length. The spatial variation of the Poisson's ratio is assumed to be negligible. As a result, the Poisson's ratio υ is considered to be a constant. Under these assumptions, the equations of equilibrium in terms of the displacement components are obtained as follows[16]:

$$(k+1)\frac{\partial^2 u}{\partial x^2}+(k-1)\frac{\partial^2 u}{\partial y^2}+2\frac{\partial^2 v}{\partial x\partial y}=0, \tag{1}$$

$$(k-1)\frac{\partial^2 v}{\partial x^2}+(k+1)\frac{\partial^2 v}{\partial y^2}+2\frac{\partial^2 u}{\partial x\partial y}=0, \tag{2}$$

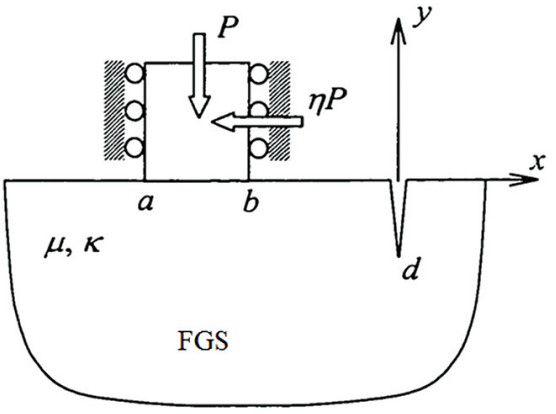

Figure 1. FGS half-plane containing surface crack in frictional sliding contact with a rigid punch of an flat profile.

where u and v are the displacement components in x and y directions, respectively and μ is the shear modulus of the half plane, k is the Kolosovs constant and for this plane strain problem, it is equal to 3-4υ. The contact mechanics problem defined above has to be solved by considering the following mixed boundary conditions[16]:

$$\sigma_{xx}(x,0)=0, \qquad x<a \ \text{ and } \ x>b \tag{3}$$

$$\sigma_{xy}(x,0)=0, \qquad x<a \ \text{ and } \ x>b \tag{4}$$

$$\frac{4\mu}{k+1}\frac{\partial}{\partial x}v(x,0)=f(x), \qquad a<x<b \tag{5}$$

$$\sigma_{xy}(x,0)=\eta\sigma_{yy}(x,0) \qquad a<x<b \tag{6}$$

$$\int_a^b \sigma_{yy}(x,0)dx=-P, \tag{7}$$

$$\sigma_{xx}(0,y)=0, \qquad d<y<0 \tag{8}$$

$$\sigma_{xy}(0,y)=0, \qquad d<y<0 \tag{9}$$

f (x) is a known function dictated by the profile of the rigid punch. In addition, the solution of the problem must satisfy the regularity conditions at infinity, requiring that all field quantities should be bounded as infinity.

The stresses and displacements for the coupled problem may then be expressed as:

$$\sigma_{ij}(x,y)=\sigma_{ij}^{(1)}(x,y)+\sigma_{ij}^{(2)}(x,y), \qquad i,j=x \text{ or } y \tag{10}$$

$$u(x,y)=u^{(1)}(x,y)+u^{(2)}(x,y), \tag{11}$$

$$v(x,y)=v^{(1)}(x,y)+v^{(2)}(x,y), \tag{12}$$

Problem 1 is the contact problem without crack and in this case the stresses and displacements will be obtained in terms of the unknown contact stress. In problem 2 stress and displacement fields will be obtained in terms of two unknown functions. The total stress and displacement fields for the original problem can then be obtained by summing the solutions of the problems 1 and 2 and satisfying the boundary conditions of the original coupled problem. Since the expressions for the contact and crack problems are derived, stresses and normal displacement derivative with Hookes Law for the coupled crack and contact problem can now be obtained in the following form[16]:

$$\sigma_{xx}(0,y)=\frac{1}{\pi}\int_d^0\left(\frac{1}{t-y}+\frac{1}{t+y}+\frac{2t}{(t+y)^2}-\frac{4t^2}{(t+y)^3}\right)f_1(t)dt + \frac{2}{\pi}\int_a^b\frac{\eta t^3-yt^2}{(y^2+t^2)^2}f_3(t)dt, \qquad -\infty<y<0, \tag{13.a}$$

$$\sigma_{xy}(0,y)=\frac{1}{\pi}\int_d^0\left(\frac{1}{t-y}+\frac{1}{t+y}+\frac{2t}{(t+y)^2}-\frac{4t^2}{(t+y)^3}\right)f_2(t)dt + \frac{2}{\pi}\int_d^0\frac{-\eta yt^2+y^2t}{(y^2+t^2)^2}f_3(t)dt, \qquad -\infty<y<0, \tag{13.b}$$

$$\frac{4\mu}{k+1}\frac{\partial}{\partial x}v(x,0) = -\frac{4}{\pi}\int_d^0 \frac{t^2 x}{(x^2+t^2)^2} f_1(t) + \frac{4}{\pi}\int_d^0 \frac{t^3}{(x^2+t^2)} f_2(t)dt - \eta\frac{k-1}{k+1} f_3(x) + \frac{1}{\pi}\int_a^b \frac{f_3(t)}{t-x}dt, \quad -\infty < x < \infty \tag{13.c}$$

Where $f_1(t)$, $f_2(t)$ and $f_3(t)$ are unknown functions. The kernels are given by:

$$K_{11}(t,y) = K_{22}(t,y) = \frac{1}{t+y} + \frac{2t}{(t+y)^2} - \frac{4t^2}{(t+y)^3}, \tag{14.a}$$

$$K_{13}(t,y) = \frac{2(\eta t^3 - yt^2)}{(y^2+t^2)^2} \tag{14.b}$$

$$K_{23}(t,y) = \frac{2(-\eta y t^2 + y^2 t)}{(y^2+t^2)} \tag{14.c}$$

$$K_{13}(t,y) = \frac{2(\eta t^3 - yt^2)}{(y^2+t^2)^2} \tag{14.d}$$

$$K_{32}(t,x) = \frac{4t^3}{(x^2+t^2)^2} \tag{14.e}$$

The singular behavior of the unknown functions will be examined using a function-theoric method. In this analysis, there are two cases. If b<0, in addition to the Cauchy singularities only terms that can become singular are K_{11} and K_{22}. Other kernels are bounded at all points of their respective intervals. If b=0, all of the kernels have to be examined to determine the singular behaviour of unknown function[7].

A numerical solution procedure based on the expansion–collocation method is developed so as to solve the singular integral equation (Equation (13)) in conjunction with the equilibrium condition given by Equation 7. Solution, it is possible to express transform unknown functions an infinite series in terms of the Jacobi polynomials.

For example in the case of flat punch problems and b<0[16]:

$$m_1(r) = (1-r)^{-1/2}\sum_{n=0}^{\infty} A_n P_n^{(-1/2,0)}(r), \tag{15.a}$$

$$m_2(r) = (1-r)^{-1/2}\sum_{n=0}^{\infty} B_n P_n^{(-1/2,0)}(r), \tag{15.b}$$

$$m_3(r) = (1-r)^{\beta}(1+r)^{\omega}\sum_{n=0}^{\infty} C_n P_n^{(\beta,\omega)}(r). \tag{15.c}$$

In this case following transformation are used,

$$m_1(r) = \frac{b-a}{P} f_1\left(\frac{d}{2}r + \frac{d}{2}\right), \tag{16.a}$$

$$m_2(r) = \frac{b-a}{P} f_2\left(\frac{d}{2}r + \frac{d}{2}\right), \tag{16.b}$$

$$m_2(r) = \frac{b-a}{P} f_2\left(\frac{d}{2}r + \frac{d}{2}\right), \tag{16.c}$$

P_n is the Jacobi polynomial, A_n, B_n and C_n are unknown constants. ω and β stand for the strengths of the singularities at the end points x = b and x = a, respectively. The expressions for these exponents are derived through the function-theoretic analysis and given as follows[16]:

$$\cot(\pi\beta) = -\eta\frac{k-1}{k+1}, \tag{17.a}$$

$$\cot(\pi\omega) = \eta\frac{k-1}{k+1}. \tag{17.b}$$

In the numerical solution, the infinite series given by Equation 15 is truncated at N. The truncated form is substituted into Equations 13 and 7. A collocation approach is used to convert Equations 13 and 7 into a system of linear algebraic equations in terms of the constant coefficients. After solving the system of linear algebraic equations for A_n, B_n and C_n contact stresses can be obtained using equation (15.c) and normalized stress intensity factor for mod I and Π can be expressed as follow[16]:

$$\frac{k_1\sqrt{-d}}{P} = \frac{-d}{(b-a)}\sum_{n=0}^{N} A_n P_n^{(-1/2,0)}(1), \tag{18.a}$$

$$\frac{k_2\sqrt{-d}}{P} = \frac{-d}{(b-a)}\sum_{n=0}^{N} B_n P_n^{(-1/2,0)}(1). \tag{18.b}$$

3. Finite Element Analysis

Besides the analytical model described in the previous section, a finite element model was developed with the general purpose finite element software ABAQUS to study the contact problem between a FGS substrate, comprised of layers of different elastic properties stacked orthogonally to contact interface, and a flat punch.

As will be shown in the next section, a very good agreement is obtained between the results obtained by the analytical and finite element methods which are indicative of the high levels of accuracy attained by these two separate techniques. The functionally graded medium is discretized by using 8-noded quadrilateral CPE8R elements. This finite element mesh contains a total of 7020 elements. As shown in Figures 2, B; H and W, respectively, denote the width of the rigid punch, the height of the graded medium and the width of the graded medium. Since the graded elastic medium is modelled as a half-plane in the analytical solution, these dimensions are selected

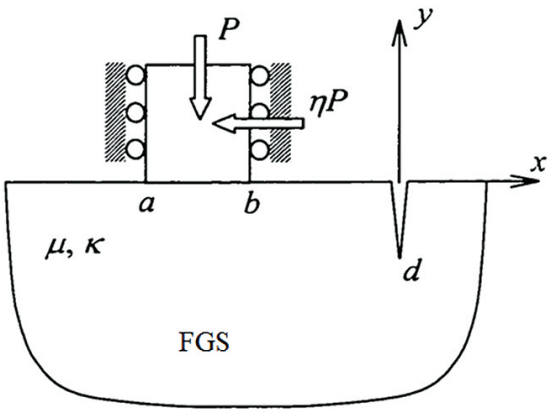

Figure 2. Boundary condition and dimension of problems.

such that the boundaries of the elastic medium would have no influence on the contact stresses. Hence, B/W is taken as 1/20 and H/W is set as 1/2. Moreover, the finite element mesh density is increased significantly in the vicinity of the contact region so as to accurately capture the sharp variations of the stress components especially near the ends of the contact zone. The deformed shape and opening crack of the finite element mesh during loading has been shown in Figure 3.

4. Results and Discussion

This section presents the numerical results obtained using the analytical model described in Section 2 and the finite element model described in Section 3. Figures 4, 5. compares the normalized contact stress distributions and normalized stress intensity factor at the crack tip with respect to the normal load pressing the punch against the substrate obtained by the analytical model and ABAQUS. Figures 6a, b. shows the distribution of normalized contact stress s_{yy} generated in the case of frictional contact between a flat punch and a graded substrate for different values of friction coefficient η.the contact stresses are infinite at the ends of the contact area except for the case η=0, for which there is no singularity at the end x=0. Contact stresses for different values of (a-b)/d are shown in Figures 6c, d. Contact stresses are singular at the end points of the contact area.

The effect of the punch location on mod I and mod II stress intensity factor for a flat punch is shown in Figures 7a, b. in these figures (a-b)/d is kept constant as 10 and υ=0.28, and stress intensity factors are given

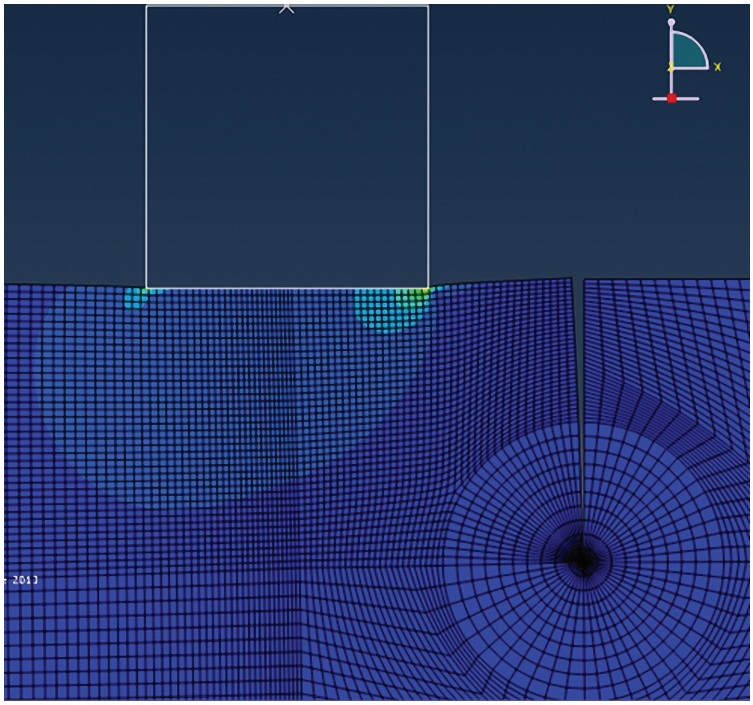

Figure 3. The Deformed shape and opening crack of the finite element mesh.

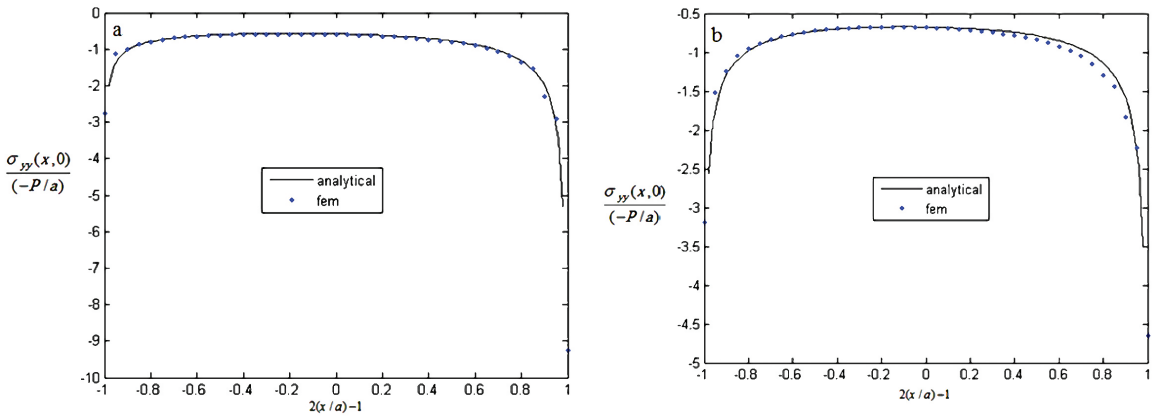

Figure 4. Comparisons of normalized contact stress distributions computed with the analytical model and ABAQUS for the case of a flat punch: (a) η=0.8, ν=0.28, a/d=1, b=0; (b) η=0.6, ν=0.28, a/d=1, b=0.

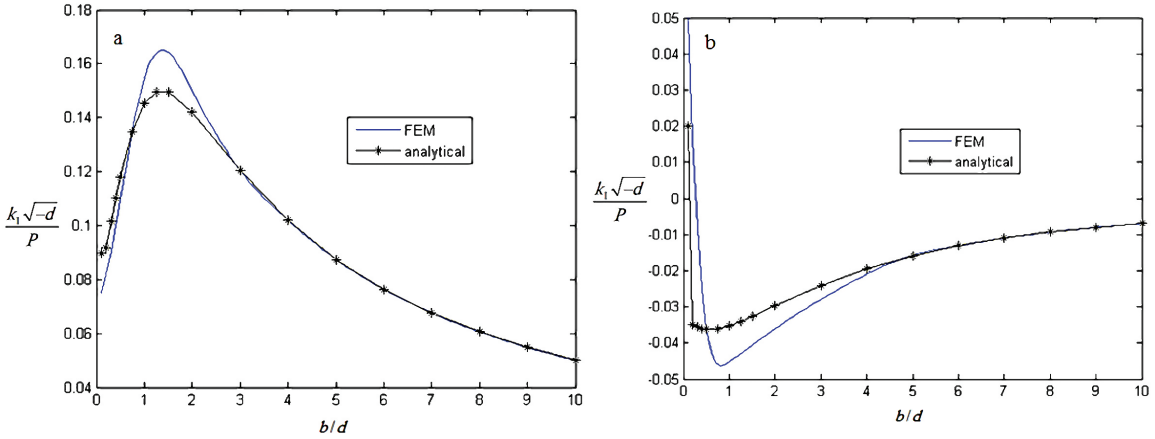

Figure 5. Comparisons of normalized stress intensity factors computed with the analytical model and ABAQUS for the case of a flat punch η=0.8, ν=0.28, (a-b)/d=1: (a) mod I; (b) mod Π.

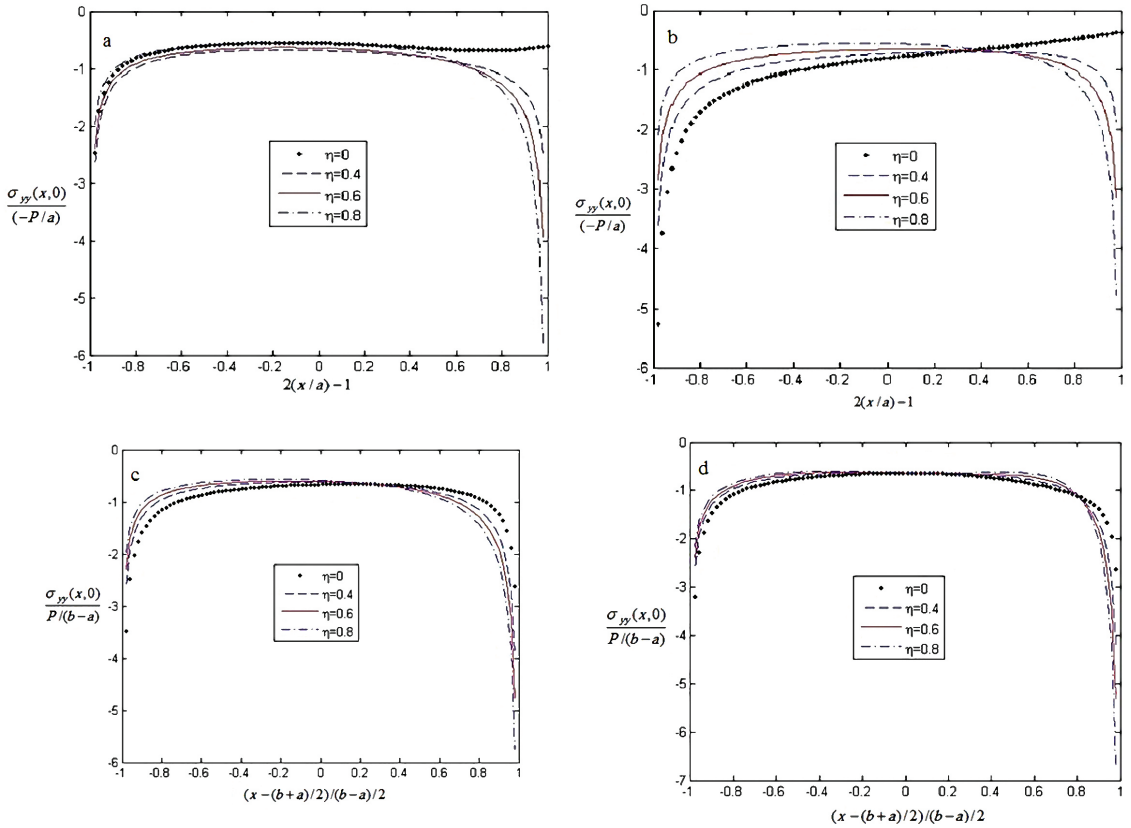

Figure 6. Normalized contact stress distributions computed for various values of the coefficient of friction by considering a flat punch: (a) b=0, υ=0.28, d/a=0.4; (b) b=0, υ=0.28, a/d=0.4; (c) (a-b)/d=1,υ=0.28, b/d=0.4; (d) (a-b)/d=10, υ=0.28, b/d=0.4.

for different values of b/d. Since, stress intensity factors are normalized with respect to d, the effect of the punch location b on stress intensity factors can be clearly observed in these figures. As b/a increases from 0, mode I stress intensity factors initially increase and they go through a peak for larger values of friction coefficient η. further increase in b/d results in a decline in mode I stress intensity factors and they approach zero for larger values of b/d which is the expected result. Similary, mod Π stress intensity factors approach zero, for larger values of b/d. It can also be seen that, if there is no tangential force, i.e., η=0, mod I stress intensity factors are negative and mod Π stress intensity factors are positive for all values of b/d.

The effect of the contact area (a/d) respect to the friction coefficient on the mod I and mod Π stress intensity factors

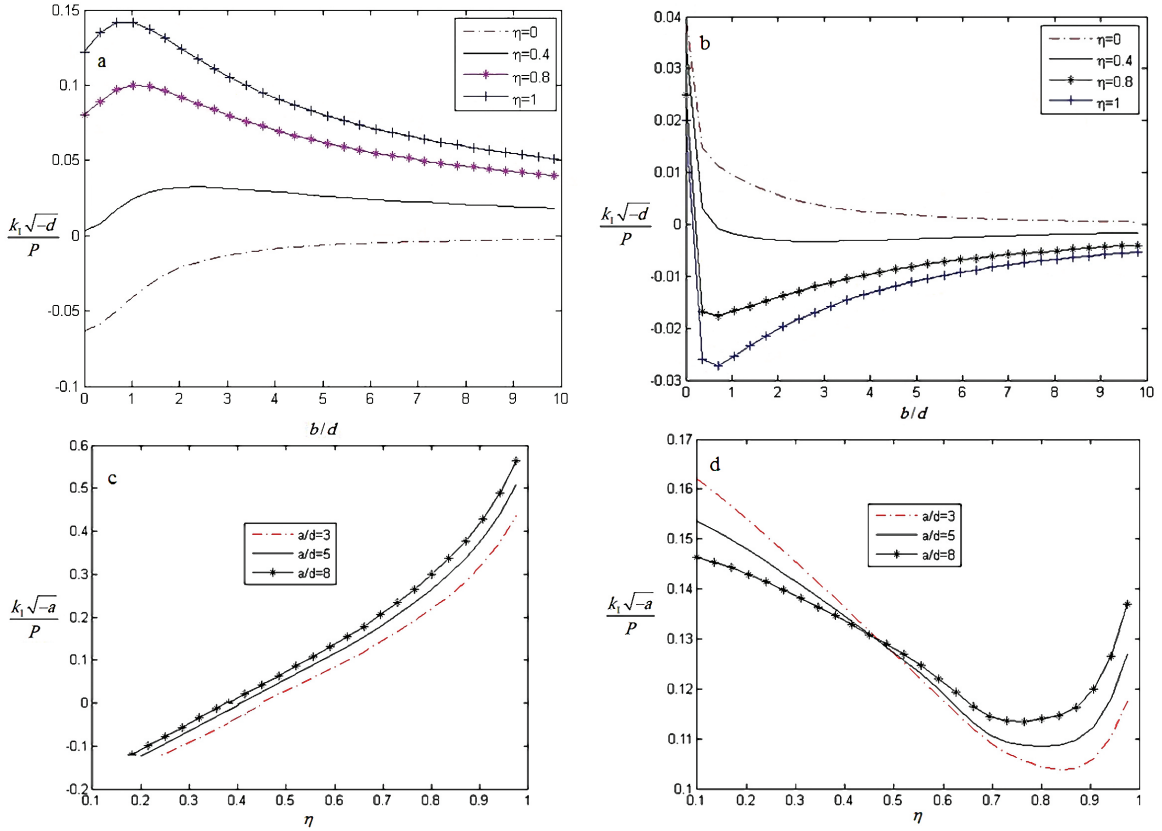

Figure 7. Normalized stress intensity factor distributions generated by considering a flat punch: (a) mod I for (a-b)/d=10, υ=0.28; (b) mod Π for (a-b)/d=10, υ=0.28; (c) mod I for b=0, υ=0.28; (d) mod Π for b=0, υ=0.28.

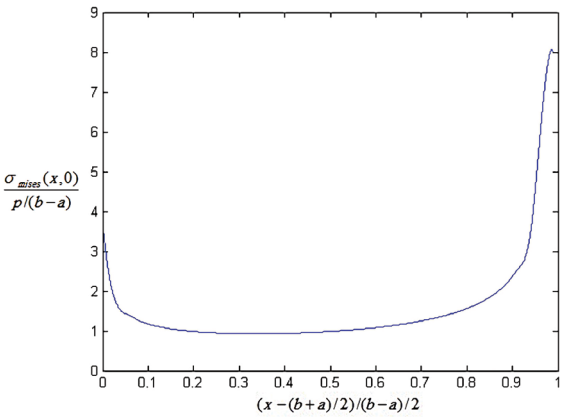

Figure 8. Shows Von Mises stress in contact area compute with FEM for $(a-b)/d=1, \upsilon=0.28, \eta=0.8$.

for b=0 is shown in Figures 7c, d. All plots were obtained for a gradation leading to a Poisson's ratio 0.28.

Failure may occur either because stresses developed in the contact region become higher than the yield limit or because stress intensity factor equals the critical stress intensity factor. Let us denote as $P_{cr}^{(1)}$ and $P_{cr}^{(2)}$, respectively, the critical normal loads at which plastic deformations may occur and crack can propagate. Figure 8 shows Von Mises stress in contact area compute with FEM, assume that when minimum Von Mises stress in contact area equal to yield stresses of functionally graded steels, area under contact can be yield. The critical load at which fracture can propagate and compute with analytical model and Critical stress intensity factor. Tables 1 and 2 presents numerical results for αβγ and γMγ gradations[15] obtained by setting the friction coefficient η equal to 0.8 and 0.4, respectively. Figures 9, 10 shows the normalized stress intensity factor and normalized critical stress intensity factor for the abγ and γMγ composite and original ferrite and original austenite steel ploted for friction coefficient η equal to 0.8 and 0.4, respectively. if critical load $P_{cr}^{(2)}$ is lower than critical load $P_{cr}^{(1)}$, failure is caused by crack growth, and if critical load $P_{cr}^{(2)}$ is lower than critical load $P_{cr}^{(1)}$, failure is caused by yield contact.

The yield limit of composite γMγ is higher than that of composite abγ. However, the minimum critical normal load (i.e. the minimum load between $P_{cr}^{(1)}$ and $P_{cr}^{(2)}$) of composite αβγ computed for η=0.8 is higher than that computed for the γMγ composite. The reverse behavior is observed for η=0.4. This indicates that the minimum critical normal load depends on punch geometry/dimensions, crack position and length, yield limit, fracture toughness and coefficient of friction. Remarkably, the minimum critical normal load of the graded constructions is almost two times as large as the critical normal load of original ferritic or austenitic phases.

Table 1. Mechanical properties and critical normal loads for $\eta = 0.8, (a-b)/d = 1$.

$P_{cr}^{(2)}$ (N)	$k_{IC} / P_{cr}^{(1)}$	$J_{IC}(kNm^{-1})$	Yield stress	$P_{cr}^{(1)}$ (N)	Composite/steel
$460\times10^6 N$	0.1442	21.8	440*mpa*	480×10^6	αβγ
$337\times10^6 N$	0.0711	11.6	690*mpa*	710×10^6	γ*M*γ
-	0.171	9	245*mpa*	260×10^6	α
-	0.4875	50	200*mpa*	215×10^6	γ

Table 2. Mechanical propertes and critical normal loads for $\eta = 0.4, (a-b)/d = 1$.

$P_{cr}^{(2)}$ (N)	$k_{IC} / P_{cr}^{(1)}$	$J_{IC}(kNm^{-1})$	Yield stress	$P_{cr}^{(1)}$ (N)	Composite/steel
-	0.1442	21.8	440*mpa*	810×10^6	αβγ
1150×10^6	0.0711	11.6	690*mpa*	1200×10^6	γ*M*γ
-	0.171	9	245*mpa*	480×10^6	α
-	0.4875	50	200*mpa*	400×10^6	γ

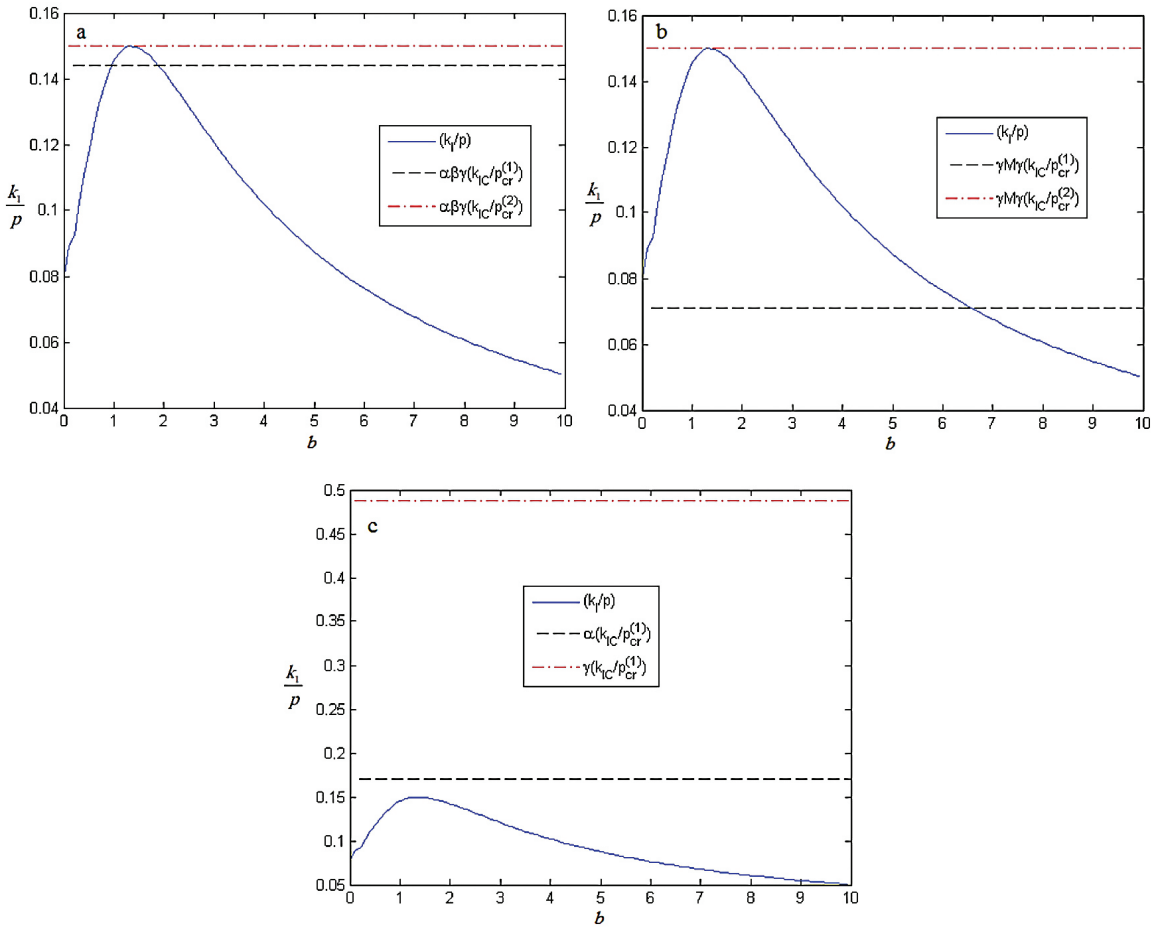

Figure 9. Normalized mode I stress intensity factors and normalized critical stress intensity factor for (a-b)/d=1, η=0.8, d=1: (a) composite αβγ; (b) composite γMγ; (c) original ferrite α and original austenite γ.

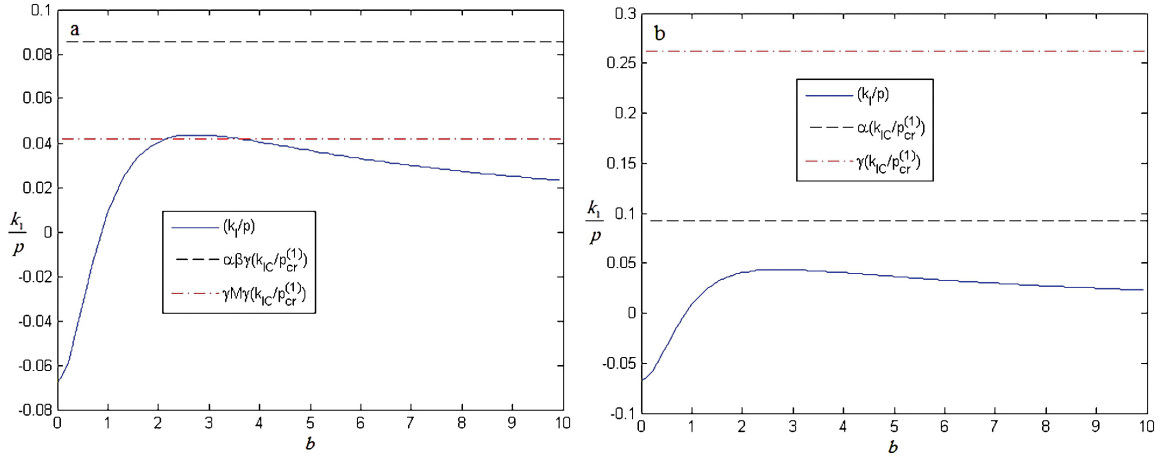

Figure 10. Normalized mode I stress intensity factors and normalized critical stress intensity factor for (a-b)/d=1, η=0.8, d=1: (a) composite αβγ and composite γMγ ; (b) original ferrite α and original austenite γ.

4. Conclusion

This study presented a parametric study on the 2-D nonlinear partial slip contact between a graded half plane (in the normal direction to contact interface) and a rigid flat punch subject to normal load. Functionally graded steels (FGS) recently produced from austenitic stainless steel and carbon steel by means of electro slag refining (ESR) were analyzed. The effect of friction coefficient on contact stresses and stress intensity factors was evaluated. For that purpose, an analytical model was developed that is in good agreement with a model implemented in the commercial finite element code ABAQUS. Remarkably, graded material constructions show critical loads two times as large as those of original ferrite and original austenite steels.

References

1. Suresh S and Mortensen A. *Fundamentals of Functionally Graded Materials*. Cambridge: The University Press; 1998.
2. Lorenzo C, Lefevre-Schlick F, Bouaziz O, Wang X, Solberg JK and Embury D. The mechanical response of compositionally graded materials. *Materials Science and Engineering A*. 2008; 483-484:266-269.
3. Moya JS, Bartolome JF, Diaz M and Requena J. Mullite/molybdenum composites. *Composite Interfaces*. 1998; 6(4):325-342. http://dx.doi.org/10.1163/156855498X00342.
4. Aghazadeh Mohandesi J and Shahosseinie MH. Transformation characteristics of functionally graded steels produced by electroslag remelting. *Metallurgical and Materials Transactions A*. 2005; 36(12):3471-3476. http://dx.doi.org/10.1007/s11661-005-0020-8.
5. Aghazadeh Mohandesi J, Shahosseinie MH and Parastar Namin R. Tensile behavior of functionally graded steels produced by electroslag remelting. *Metallurgical and Materials Transactions A*. 2006; 37A:2125-2132.
6. Nazari A, Aghazadeh Mohandesi J, Hamid Vishkasogheh M and Abedi M. Simulation of impact energy in functionally graded steels. *Computational Materials Science*. 2011; 50(3):1187-1196. http://dx.doi.org/10.1016/j.commatsci.2010.11.019.
7. Nazari A, Aghazadeh Mohandesi J and Riahi S. Fracture Toughness of Functionally Graded Steels. *Journal of Materials Engineering and Performance*. 2012; 21(4)558-563. http://dx.doi.org/10.1007/s11665-011-9945-9
8. Nazari A and Aghazadeh Mohandesi J. Modeling tensile strength of oblique layer functionally graded austenitic steel. *Computational Materials Science*. 2011; 50(4):1425-1431. http://dx.doi.org/10.1016/j.commatsci.2010.11.029.
9. Nazari A and Riahi S. Effect of layer angle on tensile behavior of oblique layer functionally graded steels. *Turkish Journal of Engineering & Environmental Sciences*. 2010; 34:17-24.
10. Nazari A, Aghazadeh Mohandesi J and Tavareh S. Microhardness profile prediction of a graded steel by strain gradient plasticity theory. *Computational Materials Science*. 2011; 50(5):1781-1784. http://dx.doi.org/10.1016/j.commatsci.2011.01.014.
11. Nazari A, Aghazadeh Mohandesi J and Tavareh S. Modeling tensile strength of austenitic graded steel based on the strain gradient plasticity theory. *Computational Materials Science*. 2011; 50(5):1791-1794. http://dx.doi.org/10.1016/j.commatsci.2011.01.016.
12. Jitcharoen J, Padture NP, Giannakopoulos AE and Suresh S. Hertzian-crack suppression in ceramics with elastic-modulus-graded surfaces. *Journal of the American Ceramic Society*. 1998; 81(9):2301-2308. http://dx.doi.org/10.1111/j.1151-2916.1998.tb02625.x.
13. Choi HJ. Effects of graded layering on the tip behavior of a vertical crack in a substrate under frictional Hertzian contact. *Engineering Fracture Mechanics*. 2001; 68(8):1033-1059.
14. Dag S and Erdogan F. A surface crack in a graded medium loaded by a sliding rigid stamp. *Engineering Fracture Mechanics*. 2002; 69(14-16):1729-1751. http://dx.doi.org/10.1016/S0013-7944(02)00053-X.
15. Aghazadeh Mohandesi J, Nazari A, Vishkasogheh MH and Abedi M. Modeling fracture toughness of functionally graded steels in crack divider configuration, modelling simul. *Materials Science and Engineering*. 2010; 18:075007. http://dx.doi.org/10.1088/0965-0393/18/7/075007.
16. Dağ S. *Crack and Contact Problems in Graded Materials: Formulations and Solution Techniques*. Saarbrücken: Müller; 2009.